



1 Development of a winter wheat model in the Community Land Model (version 4.5)

2

3 Yaqiong Lu^{1,2*}, Ian N. Williams¹, Justin E. Bagley¹, Margaret S. Torn¹, Lara M.
4 Kueppers¹

5

6 ¹*Climate and Ecosystem Sciences Division, Lawrence Berkeley National Laboratory*

7 ²*Climate and Global Dynamics Laboratory, National Center for Atmospheric Research*

8 *Corresponding author: Yaqiong Lu, yaqiong@ucar.edu, 303-497-1389, 1850 Table
9 Mesa Drive, Boulder, CO 80305

10

11 Abstract

12

13 Winter wheat is a staple crop for global food security, and is the dominant vegetation
14 cover for a significant fraction of earth's croplands. As such, it plays an important role in
15 carbon cycling and land-atmosphere interactions in these key regions. Accurate
16 simulation of winter wheat growth is not only crucial for future yield prediction under
17 changing climate, but also for understanding the energy and water cycles for winter
18 wheat dominated regions. We developed a new winter wheat model in the Community
19 Land Model (CLM) to better simulate wheat growth and grain production. These
20 included schemes to represent vernalization, as well as frost tolerance and damage. We
21 calibrated three key parameters (minimum planting temperature, maximum crop growth
22 days, and initial value of leaf carbon allocation coefficient) and modified the grain carbon
23 allocation algorithm for simulations at the U.S. Southern Great Plains ARM site (US-
24 ARM), and validated the model performance at three additional sites across the
25 continental US. We found that the new winter wheat model improved the prediction of
26 monthly variation in leaf area index, latent heat flux, and net ecosystem exchange during
27 the spring growing season. The model accurately simulated the interannual variation in
28 yield at the US-ARM site, but underestimated yield at sites and in regions (Northwestern
29 and Southeastern US) with historically greater yields.

30

31 Introduction

32

33 Wheat is a widely grown temperate cereal (Shewry, 2009), ranked fourth among
34 commodity crops with a global production of 711 million tonnes, and encompasses
35 13.3% of global permanent cropland as of 2013 (<http://faostat3.fao.org/home/E>). Wheat
36 provides one-fifth of the total caloric input of the world's population (Curtis et al., 2002),
37 and therefore plays an important role in global food security (Chakraborty and Newton,
38 2011; Vermeulen et al., 2012). In many regions, such as the United States, winter wheat
39 (*Triticum aestivum*) is the dominant wheat cultivar accounting for 74% of the total U.S.
40 wheat production, based on data from the National Agricultural Statistics Service of the
41 U.S. Department of Agriculture in 2013 (<http://www.nass.usda.gov>).

42

43 Winter wheat, which is planted in fall and harvested in early summer, responds to
44 environmental stresses and influences biogeochemical cycling and the atmosphere
45 differently from summer crops. Winter wheat may suffer less from summer drought but is
46 subject to winter damage due to exposure to low temperatures and frequent freeze-thaw



47 cycles (Vico et al., 2014). Winter wheat cropland has much less soil carbon loss
48 compared to maize cropland averaged across several sites (Ceschia et al., 2010), and
49 could either be a carbon sink (Waldo et al., 2016) or source (Anthoni et al., 2004),
50 depending on the year and the location. The earlier growing season can influence surface
51 fluxes of water, energy, and momentum, and hence regional climate (Riley et al., 2009).
52 This land surface influence is particularly strong in the U.S. Southern Great Plains, where
53 winter wheat is a dominant land-cover type. For example, statistical analyses indicated
54 cooler and moister near-surface air over Oklahoma's winter wheat belt from November to
55 April compared to adjacent grassland, due to the influence of winter wheat (McPherson et
56 al., 2004). This influence highlights the importance of adequately representing winter
57 wheat in land surface models used for climate projections, in order to assess both the
58 impact of climate change on agriculture and agriculture's influence on regional climate.
59

60 The agricultural research community developed several winter wheat models during the
61 1980s, such as the Agricultural Research Council winter wheat model (ARCWHEAT)
62 (Porter, 1984; Weir et al., 1984) and the Crop Estimation through Resource and
63 Environment Synthesis winter wheat model (CERES-wheat) (Ritchie and Otter, 1985).
64 These models were designed to simulate winter wheat growth at the farm level and have
65 well-defined winter wheat growth phenology, which is a function of thermal time and day
66 length that are adjusted by vernalization and a photoperiod factor. Photosynthesis and
67 respiration processes determine the dry matter for partitioning among roots, shoots,
68 leaves, and grain. Some models (e.g., CERES-wheat) considered winter wheat loss due to
69 extreme low temperature in winter. To extend the capability of initial models to simulate
70 crop growth at regional or global scales, some agronomic crop growth models were
71 incorporated into agro-ecosystem models. For example, CERES maize and wheat growth
72 were added into Decision Support System for Agrotechnology Transfer Model (DSSAT)
73 (Jones et al., 2003). Agro-ecosystem models vary in their complexity of representation of
74 radiation transfer, photosynthesis, soil carbon and nitrogen cycling, and soil hydrology.
75 As compared in Palosuo et al. (2011), simple models simulate radiation transfer with an
76 albedo parameter, determine photosynthesis by light use efficiency, and simulate soil
77 hydrology with a simple water bucket model, while the more complex models consider
78 canopy radiative transfer, coupled photosynthesis-stomatal conductance, and soil
79 hydrology with more detailed and mechanistic parameterizations. In the recent
80 Agricultural Model Intercomparison and Improvement Project (AgMIP), both simple and
81 complex agro-ecosystem models were categorized as Global Gridded Crop Models
82 (GGCM).
83

84 The Community Land Model (CLM) (Oleson et al., 2013) is one of the GGCM models
85 included in AgMIP. It is a state-of-the-art gridded land surface model used in the
86 Community Earth System Model (Hurrell et al., 2013) that simulates biogeophysical and
87 biogeochemical processes on a spatial grid. CLM can be run online, coupled with the
88 atmosphere model, or offline at multiple spatial scales (site, regional, and global) and
89 different resolutions. One grid cell in CLM is divided into different land units (urban,
90 glacier, lake, wetland, vegetation), and the vegetation unit can consist of up to 14 natural
91 vegetation types and 64 crop types in the most recent version (a developer version of
92 CLM4.5). In order to better represent agricultural ecosystems, Levis et al. (2012)



93 introduced crop growth modules into CLM based on the AgroIBIS model (Kucharik,
94 2003). Since their introduction, the crop modules in CLM have been updated to represent
95 more crops types (maize, soybean, cotton, wheat, rice, sugarcane, tropical maize, tropical
96 soybean) and processes, such as soybean nitrogen fixation (Drewniak et al., 2013) and
97 ozone impacts on yields (Lombardozzi et al., 2015). In CLM, crop growth depends on
98 photosynthetic processes, which are limited by light, water, and nutrient availability. At
99 each time step, photosynthesis estimations provide the potential available carbon for plant
100 growth, which is adjusted by nitrogen supply and demand. The actual available carbon is
101 distributed to leaf, stem, root, and grain by carbon allocation coefficients that vary based
102 on crop growth stages. While the initial focus for incorporating crop growth into CLM
103 was as a lower boundary condition to the atmosphere, the model also predicts crop yields
104 and is participating in the AgMIP GGCM Intercomparison project (Elliott et al., 2015).

105
106 Although Levis et al.'s initial crop growth modules in CLM included a simplified
107 representation of winter wheat growth, it has never been validated and some of the key
108 winter wheat growth processes are out of date, such as vernalization (winter crops must
109 be exposed to a period of non-lethal low temperature to produce grain), or not included
110 (e.g., frost tolerance and damage). Our new winter wheat model adopted the same
111 phenology phases as the original winter wheat model in CLM, but replaced the
112 vernalization process, added the frost tolerance and damage processes, slightly modified
113 the carbon allocation algorithm, and calibrated several key parameters that affect winter
114 wheat growth. Our work focused on improving the representation of the key growth
115 processes for winter wheat in order to, 1) better simulate the land surface influence on
116 surface CO₂, water and energy exchanges in winter wheat-dominated regions, and 2)
117 accurately simulate crop growth and yield so the model can be used for winter wheat
118 yield projections.

119
120 Methods

121
122 *Site descriptions*
123

124 We calibrated the model at the Atmospheric Radiation Measurement Southern Great
125 Plains Central Facility site (US-ARM) in northern Oklahoma and validated the model at
126 three additional sites: (1) Ponca City (US-PON) (2) Curtice Walter-Berger Cropland (US-
127 CRT) and (3) the Washington State University Cook Agronomy Farm conventional
128 tillage site (CAF-CT) (Figure 1). Site simulations were forced with half-hourly site-
129 observed meteorology (temperature, humidity, precipitation, wind, and downwelling
130 solar radiation). The annual mean temperature at US-ARM is 14.76 °C and annual mean
131 precipitation is 843 mm (Table 1). Energy fluxes and meteorological observation data are
132 available since 2002. The site has well-documented crop growth and management
133 information, including crop types, planting and harvest dates, and fertilizer amount. The
134 site conducts bi-weekly leaf area index (LAI) measurements with a light wand (Licor
135 LAI-2000) during the active growing season. Using a combination of *in situ* LAI and site
136 reflectance spectrum measurements, Williams and Torn (2015) generated a daily LAI
137 product, used here to develop the winter wheat model. Six winter wheat seasons are used
138 at the US-ARM site: 2003, 2004, 2006, 2007, 2009, and 2010 (winter wheat was not

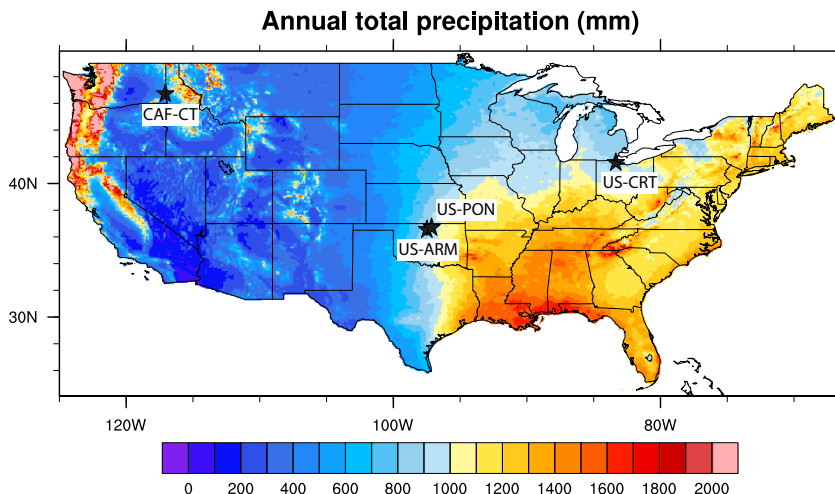


139 grown at the US-ARM site during 2005 and 2008). The US-PON site is also located in
 140 northern Oklahoma and has very similar climate as the US-ARM site (mean annual
 141 temperature is 14.94 °C and precipitation is 866 mm). At this site, observations were
 142 available for 1997-2000. Additionally, the site has LAI measurements but no crop growth
 143 documentation. The US-CRT site is located in Northern Ohio and has a cooler climate
 144 than US-ARM and US-PON. The annual mean temperature is 10.10 °C and precipitation
 145 is 849 mm. Data from this site were available for 2011-2013, but there were no LAI
 146 measurements or crop reports for winter wheat. The CAF-CT site is located in
 147 Washington state, and has lower annual precipitation (mostly in winter) and cooler
 148 climate than the other three sites (Table 1). There are also no LAI measurements
 149 available for this site.

150 Table 1. The four winter wheat sites description.

Site	Latitude	Longitude	MAT (°C)	Prec (mm)	Simulation years	References
US-ARM	36.61	-97.49	14.76	843	2002-2010	(Fischer et al., 2007)
US-PON	36.77	-97.13	14.94	866	1997-1999	(Hanan et al., 2005; Hanan et al., 2002)
US-CRT	41.63	-83.35	10.10	849	2012-2013	(Chu et al., 2014)
CAF-CT	46.78	-117.08	8.74	455	2013-2014	(Waldo et al., 2016)

151



152
 153 Figure 1. The PRISM 1981-2013 averaged annual total precipitation (mm yr^{-1}) and the
 154 four site locations (US-ARM, US-PON, US-CRT, CAF-CT) used in this study.

155

156

157 *Model development*



158

159 Similar to other crops in CLM, winter wheat has four phenological phases, including
 160 planting, leaf emergence, grain fill, and harvest. The criteria and thresholds for entering
 161 different phenology phases are listed in Table 2. Growing degree days is the key variable
 162 controlling phenology, and is measured as heat accumulation during the whole growing
 163 season or over a certain period. It was calculated by accumulating the difference (no
 164 accumulation if less than 0) between the target temperature (e.g., mean air temperature)
 165 and base temperature, and normally has a maximum daily increment. We used three
 166 different growing degree day algorithms to determine winter wheat phenology, all using
 167 the same base temperature (0 °C) and maximum daily increment (26°). The 20-year
 168 running average of growing degree days (GDD₀₂₀) uses 2-meter air temperature (T_{2m})
 169 from September to June in the northern hemisphere (from April to September in Southern
 170 Hemisphere), and is updated each year by averaging the previous 19 years. The growing
 171 degree days for soil temperature since planting (GDD_{tsoi}) uses averaged soil temperature
 172 from the top two model soil layers (0.71 cm and 2.79 cm). Growing degree days since
 173 planting (GDD_{plant}) uses T_{2m} , and is reduced by a vernalization factor (see below) after
 174 leaf emergence. To better represent winter wheat phenology, we added two additional
 175 processes: vernalization and frost damage processes.

176

177 Table 2. Criteria and notation for winter wheat to enter each phenological stage.

	Criteria	Notation
Planting	5 day running minimum temperature < minimum planting temperature and, day of year > minimum planting day of year and, 20-year running average of gdd0 > minimum gdd	$T_{5d} < 5^{\circ}\text{C}$ $doy > 1^{\text{st}}\text{ Sep}$ $GDD_{020} > 50$
Leaf emergence	Growing degree days of soil temperature to 2.79cm depth > 3% of maturity growing degree days	GDD_{tsoi} $> 3\%GDD_{mat}$
Grain fill	Growing degree days of 2m temperature since planting > 40% of maturity growing degree days	GDD_{plant} $> 40\%GDD_{mat}$
Harvest	Growing degree days of 2m temperature since planting \geq maturity growing degree days or, the number of days past planting > maximum growing days	$GDD_{plant} \geq GDD_{mat}$ $DPP > 330$

178

179 We adopted a generalized winter wheat vernalization model (Streck et al., 2003). Similar
 180 to other winter crops, winter wheat must be exposed to low and nonfreezing temperature
 181 to enter the reproductive stage. Additionally, the vernalization process affects cold
 182 tolerance, as discussed below. If plants are not fully vernalized, the potential size of the
 183 flower head will be reduced. Vernalization starts after leaf emergence and ends before
 184 flowering. To model this process, daily vernalization rate (fvn, eq. 1) is calculated based
 185 on the difference between the crown temperature (T_{crown}) and the optimum vernalization
 186 temperature (T_{opt}). In the CLM crop model, the crown temperature is the air temperature
 187 at the top of shoot. The crown temperature is typically warmer than the air temperature in
 188 winter, if the plant is covered by snow, and the same as the air temperature without snow
 189 cover. If the crown temperature is equal to the optimum temperature for a whole day,
 190 then fvn is equal to 1. Otherwise, fvn is less than 1 as calculated in eq. 1.



191
 192

$$193 \quad fvn(T_{crown}) = \begin{cases} \frac{[2(T_{crown}-T_{min})^\alpha(T_{opt}-T_{min})^\alpha - (T_{crown}-T_{min})^{2\alpha}]}{(T_{opt}-T_{min})^{2\alpha}} & T_{min} \leq T_{crown} \leq T_{max} \\ 194 \quad 0 & T < T_{min} \text{ or } T_{crown} > T_{max} \\ 1 & T_{crown} = T_{opt} \end{cases} \quad (\text{eq. 1})$$

195
 196

$$197 \quad \text{where } \alpha = \frac{\ln 2}{\ln[(T_{max} - T_{min}) / (T_{opt} - T_{min})]}$$

198
 199

200 Next, the sum of fvn over sequential days is the effective vernalization days (VD , eq. 2).

$$201 \quad VD = \sum fvn(T_{crown}) \quad (\text{eq. 2})$$

202
 203

204 This is used to calculate the vernalization factor (VF , eq. 3). VF varies from 0 to 1 (fully
 205 vernalized) to represent the vernalization stage.

$$206 \quad VF = \frac{VD^5}{22.5^5 + VD^5} \quad (\text{eq. 3})$$

207
 208

209 Finally, VF was used in adjusting the growing degree days since planting
 210 ($GDD_{plant} = GDD_{plant,unadjusted} \times VF$) and the grain carbon allocation coefficient ($a_{grain} =$
 211 $a_{grain,unadjusted} \times VF$). When winter wheat is not fully vernalized ($VF < 1$) then GDD_{plant}
 212 and a_{grain} are reduced, resulting in slowed growth and reduced yield.

213
 214

214 We quantify the impacts of low temperature damage, including from frost, using three
 215 variables: 1) temperature at which 50% of winter wheat was damaged (LT_{50}), 2) survival
 216 probability (fsurv), and 3) winter killing degree days (WDD). Here, the calculations for
 217 the three variables are briefly summarized, but more detailed descriptions of the
 218 calculations can be found in Bergjord et al., (2008) and Vico et al., (2014). LT_{50} (eq. 4)
 219 depends on LT_{50} from the previous time step (LT_{50t-1}), low temperature acclimation (i.e.
 220 hardening; RATEH), loss of hardening due to exposure to high temperatures (i.e.
 221 dehardening; RATED), stress due to respiration under snow (RATER), and exposure to
 222 low temperature (RATES). Lower LT_{50} results in greater frost tolerance for winter wheat
 223 while higher LT_{50} indicates lower frost tolerance.

224
 225

$$226 \quad LT_{50t} = LT_{50t-1} - RATEH + RATED + RATES + RATER \quad (\text{eq. 4})$$

227
 228

$$228 \quad RATEH = H_{param}(10 - \max(T_{crown}, 0))(LT_{50t-1} - LT_{50c}) \quad T_{crown} < 10^\circ\text{C} \quad (\text{eq. 5})$$

229
 230



231 The contribution of hardening to LT₅₀ was calculated as RATEH (eq. 5), which was
232 mainly a function of crown temperature (T_{crown}) and adjusted by a hardening parameter
233 (H_{param}=0.0093), maximum frost tolerance (LT_{50c}=-23 °C). RATEH increased rapidly
234 when crown temperature (T_{crown}) fell below 10 °C. When T_{crown} fell below 0 °C, the slope
235 of RATEH was same as T_{crown} at 0 °C. RATEH is also determined by the difference
236 between the current level of frost tolerance and the maximum level of frost tolerance
237 (LT_{50t-1} - LT_{50c}). At the beginning of cold acclimation, when LT_{50t-1} is much higher
238 than LT_{50c}, RAHEH increases quickly.
239

240
$$RATED = D_{param}(LT_{50i} - LT_{50t-1})(T_{crown} + 4)^3 \quad \begin{cases} T_{crown} \geq 10^\circ\text{C} \text{ when } VF < 1 \\ T_{crown} \geq -4^\circ\text{C} \text{ when } VF = 1 \end{cases} \quad (\text{eq. 6})$$

241 where LT_{50i} = -0.6 + 0.142LT_{50c} represents LT50 for an unacclimated plant
242
243

244 RATED accounts for the dehardening contribution (eq. 6), which is a function of crown
245 temperature and is adjusted by a dehardening parameter (D_{param}=2.7×10⁻⁵) and LT₅₀ for a
246 plant that is not acclimated to cold (LT_{50i}). Cold acclimation is a cumulative process and
247 can reverse (dehardening) when plants are exposed to high temperature or restart
248 (hardening) when temperature is below 10 °C. The high temperature threshold depends
249 on the vernalization stage. Dehardening occurs when T_{crown} ≥ 10°C for plants that are
250 not fully vernalized (VF<1), and when T_{crown} ≥ -4°C for plants that are fully vernalized
251 (VF=1).
252
253

254
$$RATER = R_{param} \times RE \times f(\text{snowdepth}) \quad (\text{eq. 7})$$

255 where $RE = \frac{e^{0.84+0.051T_{crown}-2}}{1.85}, R_{param} = 0.54$

256
$$f(\text{snowdepth}) = \min(\text{snowdepth}, 12.5)/12.5$$

257 Stress due to respiration under snow also increases LT₅₀ and was calculated as RATER
258 (eq. 7), which is a function of snow depth and a respiration factor (RE). RE is regression
259 function fitted to respiration measurements (Sunde, 1996). f(snowdepth) ranges from 0
260 to 1 for snow depth up to 12.5cm, and is equal to 1 when snow depth is greater than
261 12.5cm.
262
263

264
$$RATES = \frac{LT_{50t-1} - T_{crown}}{e^{-S_{param}(LT_{50t-1} - T_{crown}) - 3.74}} \quad (\text{eq. 8})$$

265 where S_{param} = 1.9

266
267

268 Long-term exposure to near lethal temperature will also increase LT₅₀ and was calculated
269 as RATES (eq. 8), which is based on the winter survival model developed by (Fowler et
270 al., 1999).
271

272 The probability of survival (fsurv, eq. 9) is a function of LT₅₀ and crown temperature.
273 The probability of survival reaches a median value when T_{crown} equals LT₅₀, and
274 increases when T_{crown} is warmer than LT50 and decreases when T_{crown} colder than LT₅₀.



275

276 $f_{surv}(T_{crown}, t) = 2^{-(\frac{|T_{crown}(t)|}{|LT50(t)|})^{asurv}}$ $T_{crown} \leq 0^\circ\text{C}$ (eq.9)

277

278 Finally, we calculate winter killing degree days (WDD, eq. 10) as a function of T_{crown} and
279 f_{surv} . WDD not only accounts for the cumulative degree days when the crop was
280 exposed to freezing temperatures but also accounts for the probability of death at the
281 temperature of exposure. High WDD occurs with low temperature and low survival
282 probability.

283

284 $WDD = \int_{winter} \max[(T_{base} - T_{crown}), 0] [1 - f_{surv}(T_{crown}, t)] dt$ (eq. 10)

285 where $T_{base} = 0^\circ\text{C}$

286

287

288 Although Bergjord et al. (2008) and Vico et al. (2014) defined the frost tolerance and
289 damage indicators described above, they did not propose a model for the growth response
290 to crop damage from low temperatures. Here we developed a hypothetical two-stage frost
291 damage parameterization that includes both instant damage and accumulated damage
292 during the leaf emergence phase of winter wheat growth. In CLM, plants tissues are
293 represented as the mass of carbon and nitrogen per m^2 ground. We simulated leaf carbon
294 and nitrogen reduction for each of the two types of frost damage. We assumed that instant
295 damage occurs at the beginning of the growing season ($VF < 0.9$) when plants are not fully
296 vernalized and have low survival probability when exposed to subzero temperatures. In
297 this case, the growth of leaves most vulnerable to cold (e.g., new leaves or small
298 seedlings) would slow or cease. After many sensitivity tests, we found the best fit to
299 observations by removing an amount of leaf carbon ($leafc_{damage_i} = 5 \text{ g C/m}^2$) to the soil
300 carbon litter pool, scaled by a factor of $1 - f_{surv}$ (eq. 11) at each time step (half-hourly).
301 The leaf carbon was reduced whenever f_{surv} was less than 1 until leaf carbon reached a
302 minimum value (10 g C/m^2).
303

304

305 $leafc_t = leafc_{t-1} - leafc_{damage_i}(1 - f_{surv})$, for $WDD > 0, f_{surv} < 1$,
306 and $leafc_t > 10$ (eq. 11)

307

308 In addition to this instantaneous damage, we introduced an accumulated damage
309 parameterization for when winter wheat is close to or has completed vernalization
310 ($VF > 0.9$) in spring. We assumed that plants would not be likely to suffer as much
311 instantaneous frost damage as in the early winter season due to less subzero temperature,
312 but that an extended period of subzero temperatures (large WDD) would lead to severe
313 crop damage. To simulate this, we let WDD accumulate up to a set value (set to 1° days),
314 when it triggers the accumulated damage function and we track the average f_{surv} for this
315 time period. When $WDD > 1^\circ$ days, all leaf carbon from previous time step ($leafc_{t-1}$,
316 representing the damage to the whole plant), scaled by a factor of $(1 - \text{averaged } f_{surv})$,
317 was removed from the leaf carbon to the soil carbon litter pool. After leaf carbon was
318 reduced, WDD was reset to 0, and the accumulation and tracking of the averaged f_{surv}
319 was restarted. For both frost damage types, leaf nitrogen was removed to the nitrogen



320 litter pool. The nitrogen was scaled to the reduction of leaf carbon by the fixed C:N ratio
 321 (25 for winter wheat). The results show that the simulation of LAI (Figure S1) can be
 322 improved by including a representation of frost damage in winter wheat models.
 323 However, the approach here is based on empirical indicators of frost damage. This
 324 suggests the potential for further improvement by incorporating process-level
 325 representation of frost damage in future model versions.
 326
 327

328 $leafc_t = leafc_{t-1} \times \text{averaged } fsurv, \text{ VF} \geq 0.9 \text{ and } WDD > 1 \text{ (eq. 12)}$

329
 330
 331
 332
 333 CLM leaf (a_{leaf}) and stem ($a_{livestem}$) carbon allocation coefficients for winter wheat were
 334 also adjusted during the grain fill to harvest phase. The original a_{leaf} and $a_{livestem}$ changed
 335 in time as a function of growing degree days. This approach resulted a rapid decline in
 336 the stem carbon allocation, and led to a grain carbon allocation coefficient that was too
 337 large (Figure S2), producing unrealistically high yields at the US-ARM site. We modified
 338 the leaf and stem carbon allocation coefficients to be functions of carbon allocation at the
 339 initial time of grain fill ($a_{leaf}^{i,3}$ and $a_{livestem}^{i,3}$), and therefore $a_{livestem}$ gradually declines and
 340 a_{grain} gradually increases during the grain fill phase (Table 3, Figure S2b). We also
 341 modified parameter values for phenological and carbon allocation functions (Table 4).
 342
 343

344
 345 Table 3. Carbon allocation algorithms for the leaf emergence to grain fill stage, and the
 346 grain fill to harvest stage.
 347

Phase	Allocation algorithm
Leaf emergence to grain fill	$a_{grain} = 0$
	$a_{froot} = a_{froot}^i - (a_{froot}^i - a_{froot}^f) \frac{GDD_{T_{2m}}}{GDD_{mat}}$
	$a_{leaf} = (1 - a_{froot}) \frac{f_{leaf}^i (e^{-0.1} - e^{[-0.1(GDD_{T_{2m}}/h)]})}{e^{-0.1} - 1}$
	$a_{livestem} = 1 - a_{grain} - a_{froot} - a_{leaf}$
Grain fill to harvest	$a_{leaf} = a_{leaf}^{i,3} \text{ when } a_{leaf}^{i,3} \leq a_{leaf}^f \text{ else}$
	$a_{leaf} = a_{leaf}^{i,3} (1 - \frac{GDD_{T_{2m}} - h}{GDD_{mat} d_L - h})^{d_{alloc}^{leaf}}$
	$a_{livestem} = a_{livestem}^{i,3} \text{ when } a_{livestem}^{i,3} \leq a_{livestem}^f \text{ else}$
	$a_{livestem} = a_{livestem}^{i,3} (1 - \frac{GDD_{T_{2m}} - h}{GDD_{mat} d_L - h})^{d_{alloc}^{stem}}$
	$a_{froot} = a_{froot}^i - (a_{froot}^i - a_{froot}^f) \frac{GDD_{T_{2m}}}{GDD_{mat}}$
	$a_{grain} = 1 - a_{livestem} - a_{froot} - a_{leaf}$



348

349

350 Table 4. A list of key parameters used for phenology and carbon and nitrogen allocation
 351 for the original and modified winter wheat models.

	Parameters	Description	Original	Modified
Phenology	minplanttemp	Minimum planting temperature	278.15 (K)	283.15 (K)
	mxmat	Maximum days for growing	265 (days)	330 (days)
	GDD _{mat}	Maturity growing degree days	1700	1700
	gddmin	Minimum growing degree days for planting	50	50
	lfemerg	Percentage of gddmaturity to enter leaf emerge phase	3%	3%
	grnfill	Percentage of gddmaturity to enter grain fill phase	40%	40%
CN allocation	a_{froot}^i	Initial value of root carbon allocation coefficient	0.3	0.3
	a_{froot}^f	Final value of root carbon allocation coefficient	0	0
	f_{leaf}^i	Initial value of leaf carbon allocation coefficient	0.425	0.6
	h	Heat unit threshold (grnfill x hybgdd)	680	680
	d_L	Leaf area index decline factor	1.05	1.05
	d_{alloc}	Leaf carbon allocation decline factor	3	3
	$d_{stemalloc}$	Stem carbon allocation decline factor	1	1

352

353 Experiment design

354

355 We set up paired CLM4.5 site simulations using Levis et al.'s original winter wheat
 356 model (CLMBASE) and our modified winter wheat model (CLMWHE) at the four winter
 357 wheat sites. We forced the site simulations with half-hourly observed temperature,
 358 relative humidity, precipitation, wind, and incoming solar radiation. Incoming longwave
 359 radiation was available at the US-ARM and US-CRT sites and was also input to the
 360 simulations at those sites. Each paired simulation ran with the same initial conditions,
 361 which were generated using a spin-up of several hundred years at each site (described
 362 below). The simulated differences between the original winter wheat and the modified
 363 winter wheat are therefore due to the modified parameters and updated processes
 364 described above.

365

366 Land surface models, especially those including biogeochemical components, require
 367 long-term (thousands of simulation years) spin-up for their carbon and nitrogen pools to
 368 reach equilibrium (Shi et al., 2013). Therefore, generating initial conditions with steady-
 369 state carbon and nitrogen pools is computationally time consuming and expensive if the
 370 simulation starts with no carbon and nitrogen. To accelerate the spin-up process, we
 371 generated site-level initial conditions by interpolating a global simulation that had
 372 reached carbon and nitrogen equilibrium, and then further spun up the site-level
 373 simulations for 200 years using recycled site observed meteorology for years listed in
 374 Table 1. When CLM reaches equilibrium, the averaged land surface variables during each
 375 atmospheric forcing cycle should not change or vary within a threshold (Table S1). We
 376 found latent heat flux, sensible heat flux, leaf area index, and wheat yield reached
 377 equilibrium fairly quickly (<40 years), but the total ecosystem carbon, total soil organic
 378 carbon, and total vegetation carbon took a longer time to reach the equilibrium state.



379

380 We also set up a regional simulation (50km resolution, 1979-2010) over the continental
381 U.S. to compare spatial patterns in yield predictions to the USDA NASS county level
382 winter wheat yield. To get the winter wheat land cover percentage, we first estimated the
383 winter wheat fraction using the USDA NASS county level acres harvested data, and then
384 split the wheat land cover percentage in the default CLM surface file into winter wheat
385 and spring wheat. Since the goal of the regional simulation was to validate the spatial
386 yield and not the carbon pools, we ran a partial spin-up and allowed the crop yield to
387 reach equilibrium while the total ecosystem carbon was not at equilibrium.

388

389 Statistical analysis of yield at US-ARM site

390

391 To determine the factors that contributed most strongly to yield in observations and the
392 model, we performed statistical regressions for US-ARM observations and CLMWHE
393 outputs separately. We had 11 observed and simulated variables including growing
394 degree days, nitrogen fertilization, peak leaf area index, precipitation, days of grain fill,
395 days of leaf emergence, day of peak leaf area index, 10cm soil moisture, 20cm soil
396 moisture, planting date, and harvest date. We performed the simple linear regressions
397 with each of these variables and compared the R² values between observational data and
398 simulation outputs.

399

400 Results

401

402 Leaf area index

403

404 The modifications to the winter wheat model improved simulation of leaf area index
405 (LAI) seasonal variation at US-ARM and US-PON sites (Figure 2). Both sites exhibited
406 reduced RMSE compared to CLMBASE (Table 6). At the US-ARM site, CLMWHE
407 underestimated peak LAI but captured the seasonal LAI variation (peak in April and then
408 decline). At the US-PON site, CLMWHE overestimated LAI throughout the growing
409 season but showed similar seasonal variation. Although US-CRT and CAF-CT sites have
410 no LAI observations, CLMWHE generally increased LAI and had a more reasonable
411 seasonal variation compared to CLMBASE.

412

413

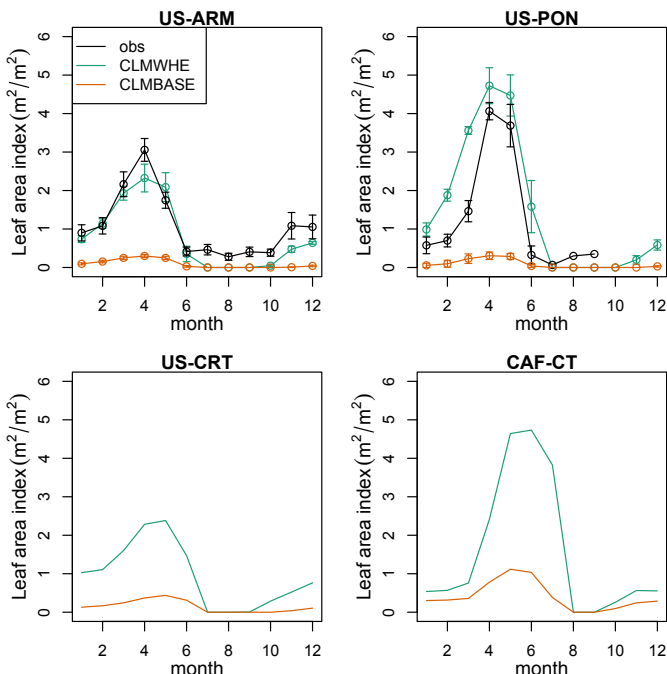
414 Table 6. Statistical comparison of leaf area index (LAI, m²/m²) between observations and
415 simulations at US-ARM and US-PON sites.

	LAI (m ² /m ²)							
	Bias		IOA		r		RMSE	
	WHE	BASE	WHE	BASE	WHE	BASE	WHE	BASE
US-ARM	-0.26	-0.99	0.85	0.5	0.76	0.72	0.71	1.29
US-PON	1.17	-1.43	0.79	0.5	0.78	0.73	1.65	2.05

416

Note: Bias, mean difference between simulation and model; IOA, index of agreement
(Willmott et al., 1985); r, Pearson's correlation coefficient; RMSE, root mean square
error. The WHE columns are the modified winter wheat model, while the BASE columns
are the original winter wheat model.

420
 421
 422
 423
 424
 425



426
 427 Figure 2. Monthly leaf area index comparison at the four sites. The error bars indicate the
 428 standard error for the month across years. There are no error bars for US-CRT and CAF-
 429 CT because the values are for one year. There are no LAI observations at US-CRT and
 430 CAF-CT.

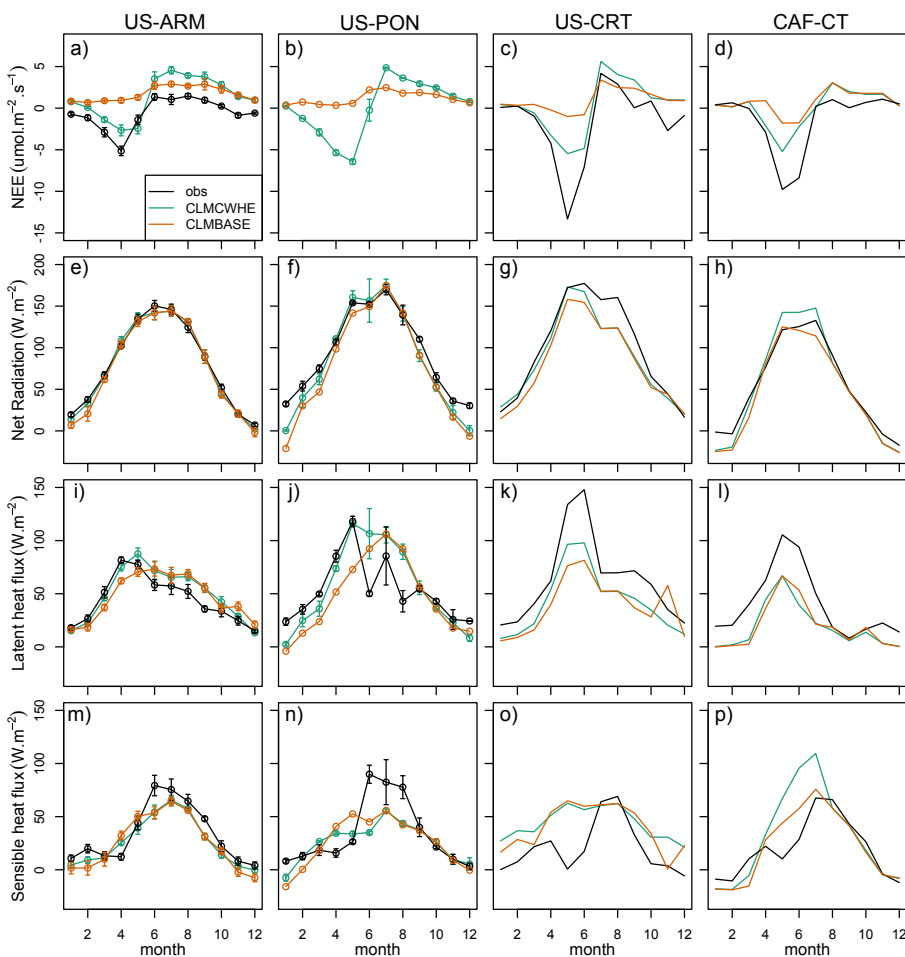
431
 432 *Surface carbon, water and energy fluxes*
 433

434 The improved simulation of LAI seasonal variation led to better monthly patterns of net
 435 ecosystem exchange of CO₂ (NEE) (Figure 3a-d). In Figure 3, negative values indicate a
 436 carbon sink, where the crop gains more carbon through photosynthesis than is lost due to
 437 respiration. During the winter wheat growing season, the observed NEE is most negative
 438 coincident with peak LAI. CLMWHE captured these seasonal patterns at US-ARM and
 439 US-CRT sites, although it did underestimate the NEE magnitudes at their peak. The
 440 underestimation of peak LAI may have contributed to this bias. CLMBASE has much
 441 smaller NEE relative to CLMWHE, consistent with the lower LAI. We also observed a
 442 discrepancy after harvest, where CLMWHE (and CLMBASE, to a lesser extent)
 443 simulated a strong carbon source for the site, but observations exhibited either neutral
 444 NEE at US-ARM or a smaller NEE at US-CRT site. This discrepancy is due to the model
 445 treating the land cover as bare ground after harvest, when in reality weeds (identified by



446 visual inspection of daily site photographs) quickly exert influence on surface fluxes of
 447 carbon.

448
 449 The annual net radiation (R_n) simulations (Figure 3e-h) at the four sites were slightly
 450 improved in CLMWHE (Figure 3e-h). Averaged across the four sites, R_n RMSE was
 451 reduced from 16.6 W.m^{-2} in CLMBASE to 12.9 W.m^{-2} in CLMWHE. The latent heat flux
 452 (LE) simulation was improved during March-May (Figure 3i-l). The spring LE RMSE
 453 was reduced by 10-70% across the four sites in CLMWHE due to the better LAI
 454 simulation in spring. However, the annual LE RMSE was only slightly reduced (up to 23%
 455 RMSE reduction in CLMWHE) at US-ARM, US-PON, and US-CRT, and showed no
 456 improvement at CAF-CT. The sensible heat flux (H) showed no obvious improvement
 457 (Figure 3m-p).
 458



459
 460 Figure 3. Monthly averaged (a)-(d) net ecosystem exchange of CO_2 ($\text{umol.m}^{-2}.\text{s}^{-1}$), (e)-(h)
 461 net radiation (W.m^{-2}), (i)-(l) latent heat flux (W.m^{-2}), and (m)-(p) sensible heat flux

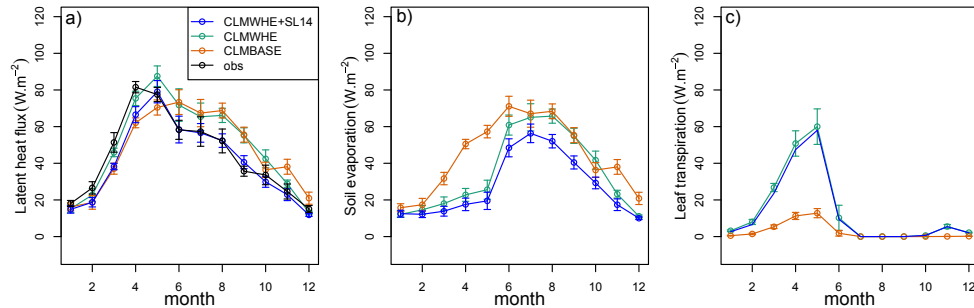


462 (W.m⁻²) for observations, CLMWHE, and CLMBASE across four sites. The US-ARM
463 site data were averaged over six winter wheat years (2003, 2004, 2006, 2007, 2009,
464 2010), US-PON data was averaged over 1997 and 1998, US-CRT data is from 2013, and
465 CAF-CT data is from 2014. The error bars indicate the standard error for the month
466 across years, and there are no error bars for US-CRT and CAF-CT because the values are
467 for one year.

468
469 At the US-ARM and US-PON sites, the LE monthly variation patterns were improved by
470 better representing leaf area index, but this improvement was limited by surface energy
471 partitioning problems in the model. The model partitioned more energy to LE than was
472 observed during the period when LAI declines in the late growing season (May-July).
473 The observed LE is 45% and 53% of net radiation at US-ARM and US-PON site, while
474 LE simulated in CLMWHE is 53% and 67% of net radiation at US-ARM and US-PON
475 site. This energy partitioning problem is reversed at the US-CRT and CAF-CT sites,
476 where the model partitioned less energy to LE than observations. The observed LE is 68%
477 and 66% of net radiation at US-CRT and CAF-CT sites, while simulated LE in
478 CLMWHE is 52% and 30% of net radiation at US-CRT and CAF-CT site. Both sites are
479 rainfed with no irrigation applied. In addition, the month of peak LE does not coincide
480 with the month of peak LAI in the observations at US-ARM and US-PON. In
481 observations, LE reaches a peak at the same time when LAI is at its peak, but in
482 CLMWHE, LE reaches peak one month later than the LAI peak. Finally, we note that the
483 winter wheat model did not improve surface energy partitioning in summer after winter
484 wheat harvest.

485
486 We found that the overestimation of LE in summer and fall can be reduced using a new
487 soil evaporation scheme (Swenson and Lawrence, 2014) that will be available in CLM5.
488 In CLM, vegetation affects LE through leaf transpiration, and LE in vegetated grid cells
489 has three components: soil evaporation, wet leaf evaporation, and dry leaf transpiration
490 (Lawrence et al., 2007). The excessive spring soil evaporation in CLM has been reported
491 in earlier versions of CLM (Lu and Kueppers, 2012; Stockli et al., 2008) and some effort
492 has been made to reduce soil evaporation. For example, Sakaguchi and Zeng (2009)
493 added a litter resistance to soil evaporation in CLM3.5 that reduced the annual averaged
494 soil evaporation. Recent work by Swenson and Lawrence (2014) added a dry surface
495 layer that increased the soil resistance and reduced soil evaporation. We tested the new
496 dry surface layer scheme at the US-ARM site, and found that soil evaporation was
497 reduced by 21% and the LE simulation was improved in May-December (Figure 4c).
498 However, the spring LE was still underestimated and the LE peak was still one month
499 later than LAI peak, which is due to the leaf transpiration reaching its peak one month
500 later than the LAI peak (Figure 4b).

501
502

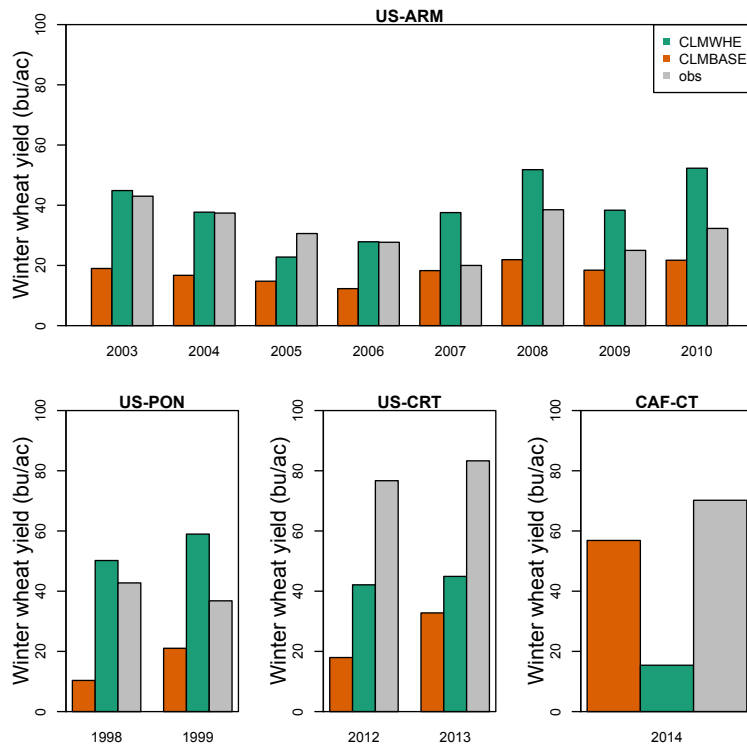


503
 504 Figure 4. US-ARM site monthly averaged (across six years) a) soil evaporation (W.m^{-2}),
 505 b) leaf transpiration (W.m^{-2}), and c) latent heat flux (W.m^{-2}). CLMWHE+SL14 is the
 506 same simulation as CLMWHE but with the new soil evaporation scheme by Swenson and
 507 Lawrence (2014).

508
 509 *Yield*
 510

511 The accuracy of the simulated yield depended on whether the region has a similar climate
 512 as the site where the model was calibrated. US-ARM had the smallest RMSE (11.88
 513 bu/ac) due to calibration, and US-PON site had only a slightly higher RMSE (16.53 bu/ac)
 514 than US-ARM because the two sites have similar climate (both located in north of
 515 Oklahoma). The yield was overestimated at the two sites by 7.34 and 14.8 bu/ac for US-
 516 ARM and US-PON. However, at US-CRT and CAF-CT, which are far away from US-
 517 ARM, the yield RMSE values were much higher (36.54 and 54.79 bu/ac) and yields were
 518 underestimated by 36.49 and 54.79 bu/ac. In terms of the interannual variation in yield,
 519 CLMWHE accurately simulated the yield decline at the US-ARM site from 2003-2006
 520 and captured the interannual variation from 2007-2010, but failed to simulate the lowest
 521 yield in 2007. We also note that CAF-CT is the only site where yield simulations with
 522 CLMWHE were worse than CLMBASE. Here the yield RMSE increased from 13.35
 523 bu/ac in CLMBASE to 54.79 bu/ac in CLMWHE (discussed further below).

524



525

526

Figure 5. The annual winter wheat yield validation against the nearest county USDA NASS yield data. The nearest county USDA NASS yield data is very similar to the site measured yield at the US-ARM site.

527

528

529

CLMWHE underestimated the US winter wheat yield by 35% compared to USDA county level yield data averaged across 1979-2010 (Figure 6), which is largely due to the underestimation of the Northwest US winter wheat yield. In the simulation, winter wheat growth in the Northwest was limited by soil water availability. Figure 7 shows that the plant wetness factor (*btran*, averaged across growing season) was <0.5 in much of the region. In CLM, *btran* varies between 0 to 1 to represent the available soil water to plant (1 means no water stress at all). The low *btran* in this region limited the photosynthesis and reduced the crop yield in the model. We applied irrigation to a single point in the Northwest, and the yield increased from 29.5 bu/ac to 80.6 bu/ac with irrigation, which is consistent with yields in subregions of the Northwest. For the Southeast US, CLMWHE simulated a similar yield as the Southern Great Plains, but the simulated yield was lower than USDA yield for the region, which may be due to model deficiencies in the representation of fertilization, lack of regional varieties, or other forms of crop management not well captured in the model.

530

531

532

533

534

535

536

537

538

539

540

541

542

543

544

545

546



547
548
549
550
551

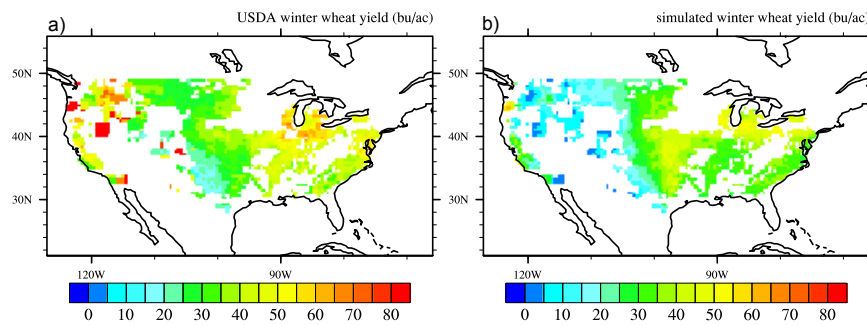


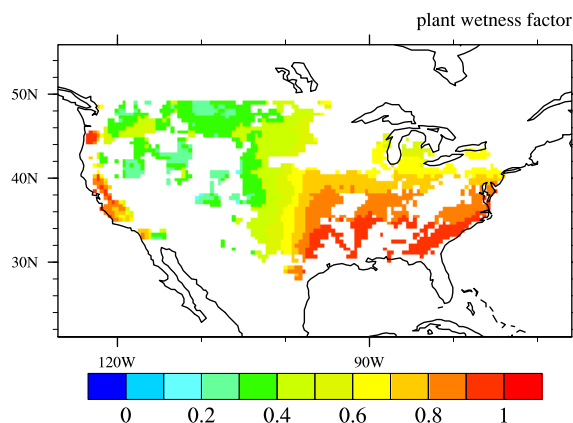
Figure 6. 1979-2010 averaged winter wheat yield for (a) USDA county level yield and (b) the simulated yield.

552
553
554
555
556
557

Figure 7. 1979-2010 averaged plant wetness factor between leaf emergence and harvest. Values less than 1 indicate water stress and cause photosynthesis to be reduced in the model.

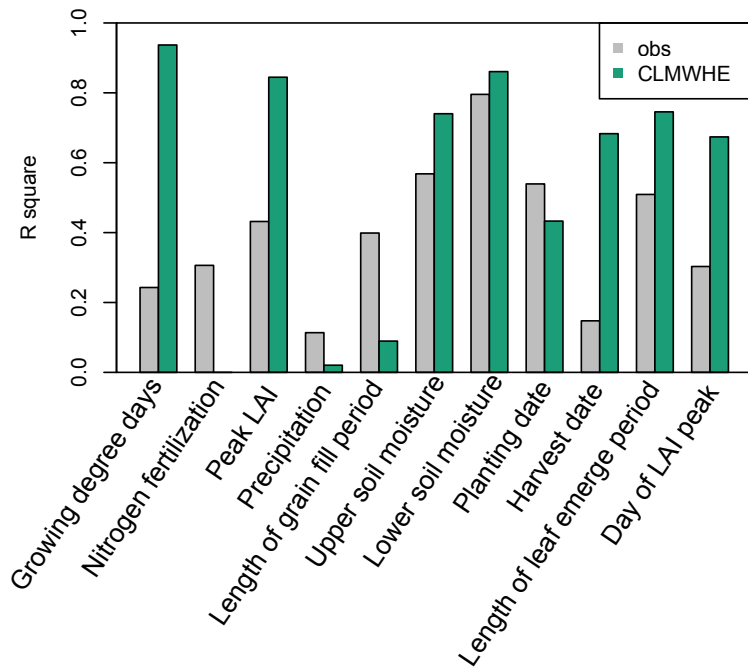
558
559
560
561
562
563
564
565
566
567
568
569
570

A simple, single variable, statistical yield regression indicated that variables important in predicting CLMWHE yield may be irrelevant for predicting observed yield. The simulated yields depend most on the growing degree days ($R^2=0.94$), which only explained 24% of observed yield variation (Figure 8). Although there are many other variables that contribute to variation in the CLMWHE yield, such as peak LAI, length of leaf emergence period, harvest date, and day of LAI peak, these variables have strong correlations with growing degree days, which suggests that crop yields in CLM depend too much on growing degree days. Soil moisture, especially the lower layer soil moisture at 20cm, is the only variable that explained a large amount of yield variation in both observations ($R^2=0.80$) and CLMWHE ($R^2=0.86$). So improved representation of soil hydrology, especially the interannual variability of soil moisture may improve the simulations of yield variation.





571
572
573



574
575 Figure 8. Comparison of the linear regression R square for yield and each of the 11
576 variables.

577

578

579 Discussion and conclusions

580

581 We improved the winter wheat model in CLM with new vernalization, frost tolerance,
582 and frost damage processes. We modified the grain carbon allocation algorithm and
583 performed a calibration on three key parameters (minimum planting temperature,
584 maximum crop growth days, and initial value of leaf carbon allocation coefficient) at the
585 US-ARM site, and then validated the model performance at three other sites in the
586 continental US. These model alterations led to large improvements for crop phenology
587 (indicated by LAI), net ecosystem exchange, and spring latent heat flux. Additionally, the
588 modeled yield RMSE is comparable to literature values (Palosuo et al., 2011). However,
589 there are several remaining limitations of the model that need to be resolved in a future
590 version.

591

592 CLM needs to better represent the land cover after harvest to include the influence of
593 weeds and litter on the carbon balance. Although CLM properly simulated the seasonal
594 evolution of NEE, the NEE RMSE at US-ARM and US-CRT (2-3 umol/m²/s) is higher



595 than the Lund-Potsdam-Jena managed Land model (LPJ-ml) simulation (Bondeau et al.,
596 2007) at the US-PON site ($1.09 \text{ umol/m}^2/\text{s}$), which is largely due to incorrect simulation
597 of NEE after harvest. When winter wheat is not alive, CLM represents the land cover as
598 bare ground so GPP is zero but heterotrophic respiration from litter and soil organic
599 matter is still large, which resulted in a carbon source after harvest (positive NEE). This
600 is not true for the US-ARM site, where we observed weed growth after harvest and
601 positive NEE (Raz-Yaseef et al., 2015). This vegetation cover after harvest resulted in a
602 near zero NEE at US-ARM or negative NEE at US-CRT site. Appropriate simulation of
603 the post-harvest land cover is critical for better representing the role of agriculture in the
604 global carbon balance.

605 CLM needs to further increase the influence of crops and vegetation on the surface
606 energy balance and latent heat flux (LE) in particular. The LE simulation in CLM has a
607 R^2 range from 0.62 to 0.97 across the four sites, which is better than other model
608 simulations at the same sites. For example, Arora et al., (2003) simulated LE RMSE 22.0 W/m^2 at US-PON from March-May in 1997 using their coupled land surface and
609 terrestrial ecosystem model (CLASS-Twoleaf model), and we simulated LE RMSE 10.55 W/m^2 at the same site from March-May averaged for 1998-1999. But our LE response to
610 the improved LAI was not as strong as we expected. Williams and Torn (2015) showed
611 that vegetation has stronger controls on surface heat flux partitioning than soil moisture at
612 the US-ARM site, where LAI explained 53% of the variation in evaporative fraction
613 ($\text{EF}=\text{LE}/(\text{LE}+\text{H})$), while soil moisture only explained 11% of EF variation. For our six
614 winter wheat years (Williams and Torn used 8 years that included other cover types), we
615 found similar patterns in the US-ARM observations. LAI explained 40% of EF variation
616 while soil moisture only explained 7% (not shown). However, EF in CLMWHE and
617 CLMBASE was not as well predicted by LAI, which only explained 5% and 1%,
618 respectively, of variation in EF. In CLM, vegetation affects LE through leaf transpiration,
619 and LE in vegetated grid cells has three components: soil evaporation, wet leaf
620 evaporation, and dry leaf transpiration (Lawrence et al., 2007). The wet leaf evaporation
621 is the smallest and overall LE depends on the tradeoff between soil evaporation and leaf
622 transpiration. Soil evaporation is dominant when LAI is small, and leaf transpiration is
623 dominant when LAI is higher. Using the US-ARM site as an example, in CLMBASE, the
624 leaf transpiration is very small due to low LAI but soil evaporation is very large, which is
625 opposite in CLMWHE (Figure 4 a and b). Such a tradeoff is why the large increase in
626 LAI in CLMWHE only increased overall LE a small amount compared to CLMBASE.
627 We found although the new soil evaporation parameterization (Swenson and Lawrence,
628 2014) in a later version of CLM reduced soil evaporation (Figure 4), the spring LE was
629 still lower than observation, which suggesting further improvements to the vegetation
630 controls on leaf transpiration are critical for accurate seasonal simulation of the latent
631 heat flux.

632 CLMWHE tends to underestimate the winter wheat yield but the yield RMSE is
633 comparable to other literature values. The averaged yield RMSE across the four sites is
634 29.09 bu/ac , which was within the range of other winter wheat models yield RMSE (21-
635 32 bu/ac) reported by (Palosuo et al., 2011), although the simulation sites and years are
636 different. The low simulated yield may be due to the insufficient calibrations. Table 4



641 listed the key crop growth parameters used in CLMWHE. We calibrated these parameters
642 at the US-ARM site, and applied the same values everywhere, which is a common
643 approach in land surface model development. However, the US-ARM site represents a
644 relatively low yield relative site compared to the U.S. national average. This likely
645 contributed to underestimated yields at sites or in regions with historically greater yields,
646 such as at US-CRT and CAF-CT, and in the Southeastern and Northwest US. The current
647 modeling framework of CLM does not facilitate the substantial calibration required to
648 more accurately capture the full range of observed winter wheat yields. As a gridded
649 global crop model, gridded parameters (e.g., maximum maturity days, leaf emerge and
650 grain fill threshold, and background litter fall factor) that allow for spatial variation in the
651 key parameters should be considered in future versions of the model. Alternately, for
652 parameters with spatial structure linked to environmental variation, parameters could
653 vary with climate or soil conditions.
654

655 We investigated the causes of the low yield in 2007 at the US-ARM site. The
656 observational yield data in Figure 4 is from the county level USDA yield estimate, which
657 is very similar ($RMSE=1.6 \text{ bu/ac}$) to the US-ARM site-observed yield. Both the site-
658 observed yield and USDA county-level yield showed the lowest values in 2007 (20
659 bu/ac), so the low yield in 2007 is not specific to the field represented by the US-ARM
660 site. The field notes indicate that only part of the wheat field was harvested in early July
661 of 2007, while the remainder of the field was not harvested due to wheat sprouting in the
662 head. Pre-harvest sprouting reduces the quality (and price) of the grain, and can occur
663 when the crop is exposed to prolonged heavy rain. We examined the precipitation,
664 temperature, and wind speed during May and June across the eight years and found that
665 in 2007 there was double the mean precipitation in June (108.2% higher than the eight-
666 year June average). Such large amounts of precipitation may have caused the low
667 observed yield. Assuming that the low yield was strongly linked to the high rainfall, the
668 implication is that the winter wheat crop model needs to include more types of
669 environmental damage to fully simulate interannual variation in yields.
670

671 Our new winter wheat model improved the LAI and yield simulation compared to the
672 original winter wheat model except at CAF-CT site due to 1) drier soil conditions during
673 the grain fill phase and 2) the adjusted grain carbon allocation coefficient in CLMWHE.
674 CLMWHE started the grain fill phase during the end of May while CLMBASE started
675 the grain fill phase in the beginning of May. In mid-May, the higher LAI in CLMWHE
676 resulted 30% more LE than CLMBASE and dried the soil. The plant wetness factor
677 dropped from 0.98 on May 15 to 0.19 on May 28 in CLMWHE, but remained greater
678 than 0.89 through May in CLMBASE. The grain carbon allocation in CLMWHE is
679 strongly limited by soil water available to the plant, so grain carbon was much smaller in
680 CLMWHE than in CLMBASE. The larger LAI also increased LE at the other three sites
681 relative to the baseline simulations, but did not result in long-term water stress due to
682 sufficient precipitation during the rainy season. The CAF-CT site has ten times less
683 precipitation than the other three sites in May. The observed LE at CAF-CT site is much
684 higher than the simulation given the same precipitation, suggesting the plant wetness
685 factor in the model is too sensitive to low precipitation.
686



687 Some of our modeling approaches need further improvements to the processes supported
688 by new observations. We developed hypothetical (empirically-based) frost damage
689 functions that account for both small and frequent damage early in the growing season,
690 and severe damage in winter and spring. Such a hypothetical approach is not uncommon
691 in crop modeling when lacking observations at a process-level. For example, CERES-
692 Wheat (Ritchie and Otter, 1985) developed a hypothetical leaf senescence scheme during
693 cold temperature that monitored a cold hardening index
694 (http://nowlin.css.msu.edu/wheat_book/CHAPTER3.html). We tested the CERES-Wheat
695 leaf senescence scheme in CLM and found it produced too much reduction on LAI. This
696 finding motivated our approach based on recently developed frost tolerance indicators.
697 The magnitude of the leaf carbon reductions and how such reductions are linked to frost
698 damage requires more observations, such as high frequency aboveground and
699 belowground biomass measurements. Furthermore, the linear yield regressions showed
700 that the yields in CLM depend too much on growing degree days, a sensitivity that is not
701 reflected in observations. In CLM, growing degree days not only determine crop
702 phenology but are also involved in calculation of the carbon allocation coefficients (Table
703 3). Exploring other possible factors that control phenology and carbon allocation may
704 improve crop simulation in CLM. Meanwhile, soil moisture, especially the deeper soil
705 moisture, explains a large amount of the yield variation in both observations and the
706 simulations. Fixing the current biases in soil hydrology and reducing interannual
707 variability in the simulated soil moisture will benefit the yield simulation.
708

709 In summary, we found that our new winter wheat model in CLM better captured the
710 monthly variation of leaf area index and improved the latent heat flux and net ecosystem
711 exchange simulation in spring. Our model correctly simulated the interannual variation in
712 yield at the US-ARM site, but the crop growth calibration at the US-ARM site introduced
713 a low-yield bias that produced underestimates of the yield in high-yield sites (US-CRT
714 and CAF-CT) and regions (Northwestern and Southeastern US). Our analysis indicates
715 that while this model of winter wheat represents a substantial step forward in simulating
716 the processes that influence winter wheat growth and yield, further refinements would be
717 helpful to capture the impacts of environmental stress on energy partitioning, carbon
718 fluxes and yield, and would improve simulations of regional variation.
719

720 Code Availability

721
722 The winter wheat code in CLM4.5 can be requested from Yaqiong Lu
723 (yaqiong@ucar.edu). And it will be available in the next released version of Community
724 Land Model (version 5) for public access.
725

726 Acknowledgements

727 This material is based upon work supported by the U.S. Department of Energy, Office of
728 Science, Office of Biological and Environmental Research, Atmospheric System
729 Research, under contract number DE-AC02-05CH11231. Funding for the US-ARM
730 AmeriFlux site was provided by the U.S. Department of Energy's Office of Science. This
731 research used resources of the National Energy Research Scientific Computing Center, a
732 DOE Office of Science User Facility supported by the Office of Science of the U.S.



733 Department of Energy under Contract No. DE-AC02-05CH11231. We acknowledge the
734 following additional AmeriFlux sites for their data records: US-ARM, US-PON, US-
735 CRT. In addition, funding for AmeriFlux data resources was provided by the U.S.
736 Department of Energy's Office of Science. We also thank Sarah Waldo and Jinshu Chi at
737 Washington State University for sharing the CAF-CT site data.

738

739

740 References:

741

- 742 Anthoni, P. M., Freibauer, A., Kolle, O., and Schulze, E. D.: Winter wheat carbon
743 exchange in Thuringia, Germany, *Agr Forest Meteorol*, 121, 55-67, 2004.
744 Arora, V. K.: Simulating energy and carbon fluxes over winter wheat using coupled land
745 surface and terrestrial ecosystem models, *Agr Forest Meteorol*, 118, 21-47, 2003.
746 Bergjord, A. K., Bonesmo, H., and Skjelvag, A. O.: Modelling the course of frost
747 tolerance in winter wheat I. Model development, *Eur J Agron*, 28, 321-330, 2008.
748 Bondeau, A., Smith, P. C., Zaehle, S., Schaphoff, S., Lucht, W., Cramer, W., Gerten, D.,
749 Lotze-Campen, H., Muller, C., Reichstein, M., and Smith, B.: Modelling the role of
750 agriculture for the 20th century global terrestrial carbon balance, *Global Change Biol*, 13,
751 679-706, 2007.
752 Ceschia, E., Beziat, P., Dejoux, J. F., Aubinet, M., Bernhofer, C., Bodson, B., Buchmann,
753 N., Carrara, A., Cellier, P., Di Tommasi, P., Elbers, J. A., Eugster, W., Grunwald, T.,
754 Jacobs, C. M. J., Jans, W. W. P., Jones, M., Kutsch, W., Lanigan, G., Magliulo, E.,
755 Marloie, O., Moors, E. J., Moureaux, C., Olioso, A., Osborne, B., Sanz, M. J., Saunders,
756 M., Smith, P., Soegaard, H., and Wattenbach, M.: Management effects on net ecosystem
757 carbon and GHG budgets at European crop sites, *Agr Ecosyst Environ*, 139, 363-383,
758 2010.
759 Chakraborty, S. and Newton, A. C.: Climate change, plant diseases and food security: an
760 overview, *Plant Pathol*, 60, 2-14, 2011.
761 Chu, H. S., Chen, J. Q., Gottgens, J. F., Ouyang, Z. T., John, R., Czajkowski, K., and
762 Becker, R.: Net ecosystem methane and carbon dioxide exchanges in a Lake Erie coastal
763 marsh and a nearby cropland, *J Geophys Res-Bioge*, 119, 722-740, 2014.
764 Drewniak, B., Song, J., Prell, J., Kotamarthi, V. R., and Jacob, R.: Modeling agriculture
765 in the Community Land Model, *Geosci Model Dev*, 6, 495-515, 2013.
766 Elliott, J., Muller, C., Deryng, D., Chryssanthacopoulos, J., Boote, K. J., Buchner, M.,
767 Foster, I., Glotter, M., Heinke, J., Iizumi, T., Izaurralde, R. C., Mueller, N. D., Ray, D.
768 K., Rosenzweig, C., Ruane, A. C., and Sheffield, J.: The Global Gridded Crop Model
769 Intercomparison: data and modeling protocols for Phase 1 (v1.0), *Geosci Model Dev*, 8,
770 261-277, 2015.
771 Fischer, M. L., Billesbach, D. P., Berry, J. A., Riley, W. J., and Torn, M. S.:
772 Spatiotemporal variations in growing season exchanges of CO₂, H₂O, and sensible heat
773 in agricultural fields of the Southern Great Plains, *Earth Interact*, 11, 2007.
774 Fowler, D. B., Limin, A. E., and Ritchie, J. T.: Low-temperature tolerance in cereals:
775 Model and genetic interpretation, *Crop Sci*, 39, 626-633, 1999.
776 Hanan, N. P., Berry, J. A., Verma, S. B., Walter-Shea, E. A., Suyker, A. E., Burba, G. G.,
777 and Denning, A. S.: Testing a model of CO₂, water and energy exchange in Great Plains
778 tallgrass prairie and wheat ecosystems, *Agr Forest Meteorol*, 131, 162-179, 2005.



- 779 Hanan, N. P., Burba, G., Verma, S. B., Berry, J. A., Suyker, A., and Walter-Shea, E. A.:
780 Inversion of net ecosystem CO₂ flux measurements for estimation of canopy PAR
781 absorption, *Global Change Biol.*, 8, 563-574, 2002.
- 782 Hurrell, J. W., Holland, M. M., Gent, P. R., Ghan, S., Kay, J. E., Kushner, P. J.,
783 Lamarque, J. F., Large, W. G., Lawrence, D., Lindsay, K., Lipscomb, W. H., Long, M.
784 C., Mahowald, N., Marsh, D. R., Neale, R. B., Rasch, P., Vavrus, S., Vertenstein, M.,
785 Bader, D., Collins, W. D., Hack, J. J., Kiehl, J., and Marshall, S.: The Community Earth
786 System Model A Framework for Collaborative Research, *B Am Meteorol Soc*, 94, 1339-
787 1360, 2013.
- 788 Jones, J. W., Hoogenboom, G., Porter, C. H., Boote, K. J., Batchelor, W. D., Hunt, L. A.,
789 Wilkens, P. W., Singh, U., Gijsman, A. J., and Ritchie, J. T.: The DSSAT cropping
790 system model, *Eur J Agron.*, 18, 235-265, 2003.
- 791 Kucharik, C. J.: Evaluation of a Process-Based Agro-Ecosystem Model (Agro-IBIS)
792 across the US Corn Belt: Simulations of the Interannual Variability in Maize Yield, *Earth
Interact.*, 7, 2003.
- 793 Lawrence, D. M., Thornton, P. E., Oleson, K. W., and Bonan, G. B.: The partitioning of
794 evapotranspiration into transpiration, soil evaporation, and canopy evaporation in a
795 GCM: Impacts on land-atmosphere interaction, *J Hydrometeorol.*, 8, 862-880, 2007.
- 796 Levis, S., Bonan, G. B., Kluzek, E., Thornton, P. E., Jones, A., Sacks, W. J., and
797 Kucharik, C. J.: Interactive Crop Management in the Community Earth System Model
798 (CESM1): Seasonal Influences on Land-Atmosphere Fluxes, *Journal of Climate*, 25,
799 4839-4859, 2012.
- 800 Lombardozzi, D., Levis, S., Bonan, G., Hess, P. G., and Sparks, J. P.: The Influence of
801 Chronic Ozone Exposure on Global Carbon and Water Cycles, *Journal of Climate*, 28,
802 292-305, 2015.
- 803 Lu, Y. Q. and Kueppers, L. M.: Surface energy partitioning over four dominant
804 vegetation types across the United States in a coupled regional climate model (Weather
805 Research and Forecasting Model 3-Community Land Model 3.5), *J Geophys Res-Atmos.*,
806 117, 2012.
- 807 McPherson, R. A., Stensrud, D. J., and Crawford, K. C.: The impact of Oklahoma's
808 winter wheat belt on the mesoscale environment, *Mon Weather Rev.*, 132, 405-421, 2004.
- 809 Oleson, K., Lawrence, D., Bonan, G., Drewniak, B., Huang, M., Koven, C., Levis, S., Li,
810 F., Riley, W., Subin, Z., Swenson, S., and Thornton, P.: Technical Description of version
811 4.5 of the Community Land Model (CLM), National Center for Atmospheric Research,
812 Boulder, CO, NCAR/TN-503+STR, 434 pp., 2013.
- 813 Palosuo, T., Kersebaum, K. C., Angulo, C., Hlavinka, P., Moriondo, M., Olesen, J. E.,
814 Patil, R. H., Ruget, F., Rumbaur, C., Takac, J., Trnka, M., Bindi, M., Caldag, B., Ewert,
815 F., Ferrise, R., Mirschel, W., Saylan, L., Siska, B., and Rotter, R.: Simulation of winter
816 wheat yield and its variability in different climates of Europe: A comparison of eight crop
817 growth models, *Eur J Agron.*, 35, 103-114, 2011.
- 818 Porter, J. R.: A Model of Canopy Development in Winter-Wheat, *J Agr Sci.*, 102, 383-
819 392, 1984.
- 820 Raz-Yaseef, N., Billesbach, D. P., Fischer, M. L., Biraud, S. C., Gunter, S. A., Bradford,
821 J. A., and Torn, M. S.: Vulnerability of crops and native grasses to summer drying in the
822 US Southern Great Plains, *Agr Ecosyst Environ.*, 213, 209-218, 2015.



- 824 Riley, W. J., Biraud, S. C., Torn, M. S., Fischer, M. L., Billesbach, D. P., and Berry, J.
825 A.: Regional CO₂ and latent heat surface fluxes in the Southern Great Plains:
826 Measurements, modeling, and scaling, *J Geophys Res-Biogeo*, 114, 2009.
827 Ritchie, J. R. and Otter, S.: Description and performance of CERES-Wheat: A User
828 oriented Wheat Yield Model. ARS Wheat Yield Project ARS-38., Springfield, MO, 159-
829 175 pp., 1985.
830 Sakaguchi, K. and Zeng, X. B.: Effects of soil wetness, plant litter, and under-canopy
831 atmospheric stability on ground evaporation in the Community Land Model (CLM3.5), *J*
832 *Geophys Res-Atmos*, 114, 2009.
833 Shewry, P. R.: Wheat, *J Exp Bot*, 60, 1537-1553, 2009.
834 Shi, M. J., Yang, Z. L., Lawrence, D. M., Dickinson, R. E., and Subin, Z. M.: Spin-up
835 processes in the Community Land Model version 4 with explicit carbon and nitrogen
836 components, *Ecol Model*, 263, 308-325, 2013.
837 Stockli, R., Lawrence, D. M., Niu, G. Y., Oleson, K. W., Thornton, P. E., Yang, Z. L.,
838 Bonan, G. B., Denning, A. S., and Running, S. W.: Use of FLUXNET in the community
839 land model development, *J Geophys Res-Biogeo*, 113, 2008.
840 Streck, N. A., Weiss, A., and Baenziger, P. S.: A generalized vernalization response
841 function for winter wheat, *Agron J*, 95, 155-159, 2003.
842 Sunde, M.: Effects of winter climate on growth potential, carbohydrate content and cold
843 hardiness of timothy (*Phleum pratense* L.) and red clover
844 (*Trifolium pratense* L.), PhD thesis, Agricultural University of Norway, 1996.
845 Swenson, S. C. and Lawrence, D. M.: Assessing a dry surface layer-based soil resistance
846 parameterization for the Community Land Model using GRACE and FLUXNET-MTE
847 data, *J Geophys Res-Atmos*, 119, 2014.
848 Vermeulen, S. J., Campbell, B. M., and Ingram, J. S. I.: Climate Change and Food
849 Systems, *Annu Rev Env Resour*, 37, 195-+, 2012.
850 Vico, G., Hurry, V., and Weih, M.: Snowed in for survival: Quantifying the risk of winter
851 damage to overwintering field crops in northern temperate latitudes, *Agr Forest Meteorol*,
852 197, 65-75, 2014.
853 Waldo, S., Chi, J. S., Pressley, S. N., O'Keeffe, P., Pan, W. L., Brooks, E. S., Huggins, D.
854 R., Stockle, C. O., and Lamb, B. K.: Assessing carbon dynamics at high and low rainfall
855 agricultural sites in the inland Pacific Northwest US using the eddy covariance method,
856 *Agr Forest Meteorol*, 218, 25-36, 2016.
857 Weir, A. H., Bragg, P. L., Porter, J. R., and Rayner, J. H.: A Winter-Wheat Crop
858 Simulation-Model without Water or Nutrient Limitations, *J Agr Sci*, 102, 371-382, 1984.
859 Willmott, C. J., Ackleson, S. G., Davis, R. E., Feddema, J. J., Klink, K. M., Legates, D.
860 R., Odonnell, J., and Rowe, C. M.: Statistics for the Evaluation and Comparison of
861 Models, *J Geophys Res-Oceans*, 90, 8995-9005, 1985.
862